Structural and biochemical investigation of two *Arabidopsis* shikimate kinases: The heat-inducible isoform is thermostable

Geoffrey Fucile,[1,†] Christel Garcia,[1] Jonas Carlsson,[2] Maria Sunnerhagen,[2] and Dinesh Christendat[1,3]*

[1]Department of Cell and Systems Biology, University of Toronto, Ontario, Canada
[2]Department of Physics, Chemistry and Biology, Linköping University, Linköping, Sweden
[3]Center for the Analysis of Genome Evolution and Function, University of Toronto, Ontario, Canada

Received 13 February 2011; Revised 8 April 2011; Accepted 8 April 2011
DOI: 10.1002/pro.640
Published online 21 April 2011 proteinscience.org

Abstract: The expression of plant shikimate kinase (SK; EC 2.7.1.71), an intermediate step in the shikimate pathway to aromatic amino acid biosynthesis, is induced under specific conditions of environmental stress and developmental requirements in an isoform-specific manner. Despite their important physiological role, experimental structures of plant SKs have not been determined and the biochemical nature of plant SK regulation is unknown. The *Arabidopsis thaliana* genome encodes two SKs, AtSK1 and AtSK2. We demonstrate that AtSK2 is highly unstable and becomes inactivated at 37°C whereas the heat-induced isoform, AtSK1, is thermostable and fully active under identical conditions at this temperature. We determined the crystal structure of AtSK2, the first SK structure from the plant kingdom, and conducted biophysical characterizations of both AtSK1 and AtSK2 towards understanding this mechanism of thermal regulation. The crystal structure of AtSK2 is generally conserved with bacterial SKs with the addition of a putative regulatory phosphorylation motif forming part of the adenosine triphosphate binding site. The heat-induced isoform, AtSK1, forms a homodimer in solution, the formation of which facilitates its relative thermostability compared to AtSK2. *In silico* analyses identified AtSK1 site variants that may contribute to AtSK1 stability. Our findings suggest that AtSK1 performs a unique function under heat stress conditions where AtSK2 could become inactivated. We discuss these findings in the context of regulating metabolic flux to competing downstream pathways through SK-mediated control of steady state concentrations of shikimate.

Keywords: shikimate; heat stress; *Arabidopsis thaliana*

Introduction

The shikimate pathway is the biosynthetic route to the production of the aromatic amino acids and many other aromatic compounds with essential functions in plants, microbes, and fungi.[1,2] Specifically, the shikimate pathway begins with the 3-deoxy-D-*arabino*-heptulosonate-7-phosphate synthase-catalyzed condensation of phosphoenolpyruvate and

Abbreviations: SK, shikimate kinase; ATP, adenosine triphosphate; cTP, chloroplast transit peptide; At, *Arabidopsis thaliana*; Al, *Arabidopsis lyrata*; Bn, *Brassica napus*; Mt, *Mycobacterium* tuberculosis; Tris, 2-amino-2-hydroxymethyl-propane-1,3-diol; DTT, dithiotreitol; RC, reduced core; NB, nucleotide binding; ESB, extended shikimate binding; RMSD, root mean square deviation.

Additional Supporting Information may be found in the online version of this article.

†Present address: Department of Molecular Biology, University of Geneva, Switzerland.

Grant sponsor: Natural Sciences and Engineering Research Council (NSERC) of Canada, Early Research Award from the Ontario provincial government (D.C.)

*Correspondence to: Dinesh Christendat, Department of Cell and Systems Biology, University of Toronto, 25 Harbord Street, Toronto, ON, Canada M5S 3G5. E-mail: dinesh.christendat@utoronto.ca

erythrose-4-phosphate, from glycolysis and the pentose phosphate pathway, respectively, and terminates with the production of chorismate.[3] Chorismate can be converted to the aromatic amino acids phenylalanine, tyrosine, and tryptophan through several enzymatic steps. Intermediates of the shikimate pathway are also considered branch point compounds for other biosynthetic pathways.[1,4] The shikimate pathway is restricted primarily to bacteria, archaea, fungi, apicomplexa parasites, and plantae.[1,5–8] However, there is evidence for genes encoding shikimate pathway enzymes in the basal metazoan *Nematostella vectensis* through horizontal gene transfer from its bacterial and eukaryotic (dinoflagellate) symbionts.[9] In plants, the aromatic amino acids are precursors for the production of phytohormones (auxins), electron carriers, enzyme cofactors (ubiquinone, plastoquinone, menaquinone, and nicotinamide adenine dinucleotide), antioxidants (tocopherol), pathogen defence compounds (camalexin, salicylate), pharmacologically important alkaloids (morphine, vinblastine), and many important phenylpropanoids (lignins, anthocyanins).[1–3] The plant shikimate pathway is also targeted by the widespread glyphosate herbicide at the penultimate step catalyzed by 5-enolpyruvylshikimate-3-phospate synthase.[10] It is, therefore, of great interest to understand how the plant shikimate pathway is regulated.

The shikimate pathway plays an important role in plant physiology and is expected to be highly regulated. Several studies have suggested a role for shikimate kinase (SK; EC 2.7.1.71) in regulating the plant shikimate pathway.[11–15] SKs catalyze the fifth enzymatic step of the shikimate pathway through the adenosine triphosphate (ATP)-dependent phosphorylation of the 3′ hydroxyl of shikimate. Evidence for a role of plant SKs in regulating flux through the shikimate pathway include the observation that SK transcripts are induced by fungal elicitors in tomato,[15] the sensitivity of SK activity to cellular ATP concentrations,[11] and the differential expression of plant SK paralogs during specific developmental stages and stress responses in both rice[13] and Arabidopsis.[14] SKs also function at a branch point to lignin biosynthesis, where shikimate is a recycled acceptor substrate in acyltransferase reactions and may play an important role in regulating phenylpropanoid flux.[16] The participation of plant SKs in metabolic regulation is further supported by the observation that most plant genomes maintain multiple SK-encoding loci.[14] We previously demonstrated that the *Arabidopsis thaliana* genome contains two genes encoding functional SK enzymes, AtSK1 (At2g21940) and AtSK2 (At4g39540), which arose following a duplication event approximately 20–60 million years ago.[14,17] The kinetic parameters of the AtSK1 and AtSK2 enzymes under standard conditions are similar and comparable to those reported for microbial SKs.[14] Therefore, it is interesting to determine whether AtSK1 and AtSK2 function redundantly, or if they perform unique functions. Consistent with the latter hypothesis, AtSK1 expression shows greater than 10-fold induction in response to heat stress, whereas AtSK2 expression remains unchanged.[14,18] The shikimate pathway is particularly relevant to the heat stress response of plants. Plants require increased flux through the shikimate pathway in response to heat stress for the production of aromatic amino acids in the synthesis of heat shock proteins (HSPs),[19] the replacement of damaged proteins, and a number of metabolites required for the protection of cells against oxidative damage including phenylpropanoids such as anthocyanin.[20–22]

In this study, we investigate the hypothesis that the heat-induced SK isoform in *Arabidopsis thaliana*, AtSK1, has a specialized function in response to heat stress. This hypothesis predicts that the activity of AtSK1 exceeds that of AtSK2 at higher temperatures. Consistent with this prediction, we demonstrate that AtSK1 activity is stable at elevated temperatures (37°C), whereas the activity and proportion of natively folded AtSK2 declines rapidly. Our findings, therefore, support a unique role for AtSK1 under heat stress conditions where AtSK2 could become inactivated in the plant. To understand this functional asymmetry, we determined the crystal structure of AtSK2, the first SK structure from the plant kingdom, and integrated biophysical characterizations with a comparative analysis of AtSK1 and AtSK2 structural variation. We discuss the functional asymmetry of AtSK1 and AtSK2 in the context of plant secondary metabolism. This model system of SK gene duplicates also provides a framework to address the largely unexplored relationship between the evolution of the regulatory properties of a protein and its structure and function.[23,24]

Results

Divergence of AtSK1 and AtSK2 primary sequences and regulation

We assessed the conservation of the SK gene duplication in *Arabidopsis thaliana* by conducting a phylogenetic analysis of SK-coding sequences from the major land plant families. The topology of plant SK gene duplicate retention is lineage specific (Supporting Information Fig. 1).[14] Ancient SK gene duplications in the monocot and *Pinaceae* families have been conserved in extant species within these clades, whereas SK gene duplication in the dicots has been primarily genus specific. The AtSK1 and AtSK2 gene duplication topology is conserved in the closely

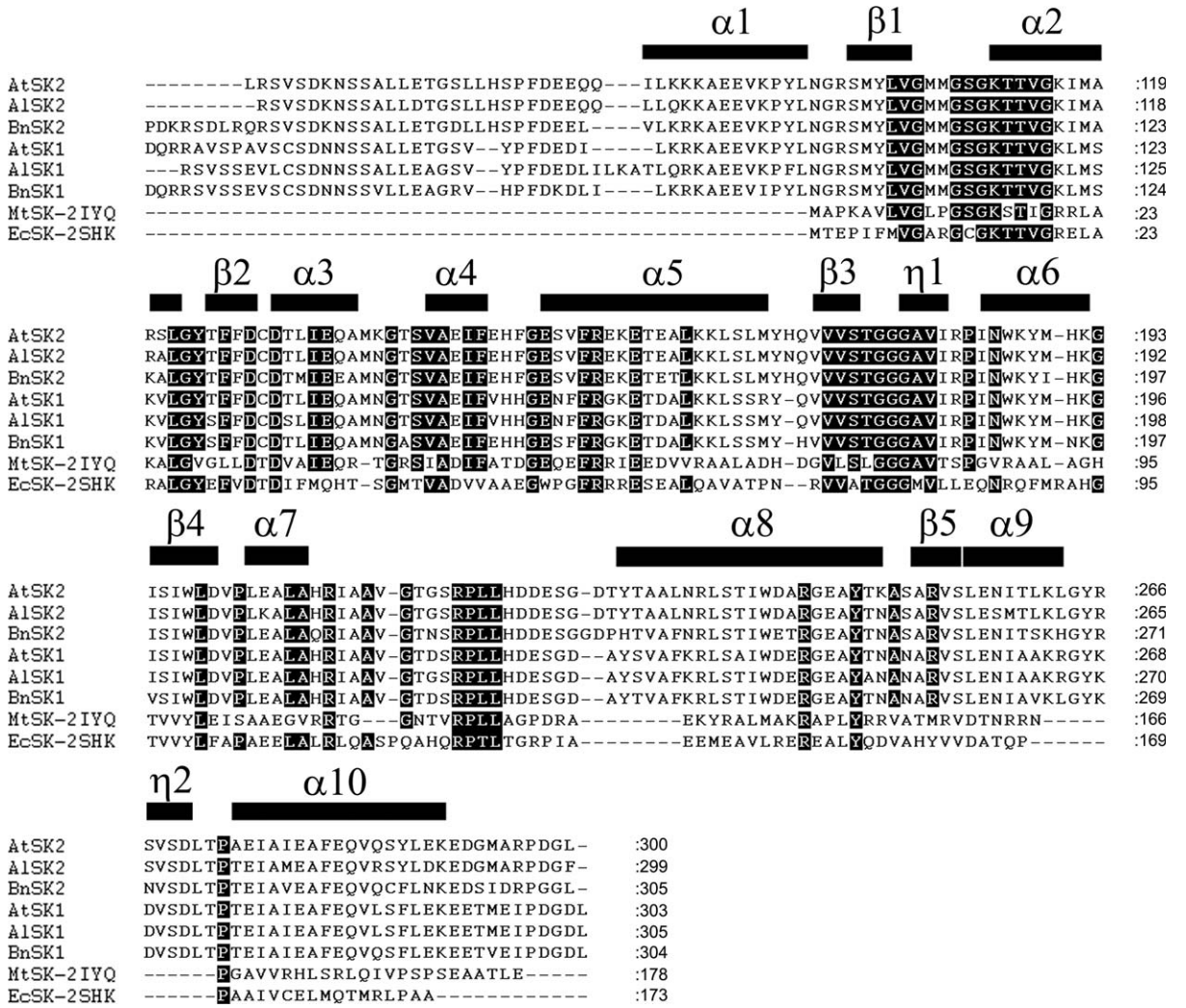

Figure 1. Multiple sequence alignment of plant SK amino acid sequences from the Brassicaceae (At, *Arabidopsis thaliana*; Bn, *Brassica napus*) and two bacteria (Mt, *Mycobacterium tuberculosis*, PDB entry 2IYQ; Ec, *Erwinia chrysanthemi*, PDB entry 2SHK). The sequence regions corresponding to secondary structures identified from the crystallographic structure of AtSK2 (PDB entry 3NWJ) are indicated (α, alpha-helix; η, 310 helix; β, beta-strand).

related species *Arabidopsis lyrata* (Al) and *Brassica napus* (Bn) of the *Brassicaceae* lineage. Multiple protein sequence alignment of the *Brassicaceae* SK duplicates shows AtSK1 is 93 and 91% identical to BnSK1 and AlSK1, respectively, and AtSK2 is 86 and 94% identical to BnSK2 and AlSK2, respectively (Fig. 1). AtSK1 and AtSK2 are ~80% identical at the amino acid level.

The gene expression patterns of the *Arabidopsis thaliana* SK isoforms, AtSK1 and AtSK2, show a signature of regulatory subfunctionalization.[14] AtSK1 expression is typically induced under conditions where AtSK2 expression has decreased, showing a moderate anticorrelation (Pearson's correlation $R = -0.33$) (Supporting Information Fig. S2). A conspicuous characteristic of the regulatory asymmetry between the Arabidopsis SK paralogs is the ~10-fold induction of AtSK1 transcript under heat stress.[14,18] AtSK1 is coexpressed with stress response-related genes, including 25 genes annotated as heat-shock related (Supporting Information Fig. S3). AtSK2 is coexpressed with genes involved in processes commonly associated to the shikimate pathway, including secondary and amino acid metabolism and chloroplast-related functions such as photosynthesis and tetrapyrrole biosynthesis.

Crystal structure of the AtSK2 protein

To date, SKs have only been characterized structurally from bacteria.[25–30] Plant SKs share at most 30% identity with these bacterial proteins. Additionally, plant SKs are known to be approximately 10 kDa larger than bacterial SKs.[11,12,31] Consistent with the other plant shikimate pathway enzymes, plants SKs possess an N-terminal chloroplast transit peptide (cTP), which is cleaved during plastid import, and have been shown to be chloroplast localized.[11–13] We determined the crystal structure of AtSK2 to characterize the differences between plant and microbial

Table I. *AtSK2 Crystallographic Model Refinement and Data Collection Statistics*

Resolution range (Å)	19.0–2.35
Number of unique reflections	16917
Completeness for range	87.7
R_{fact}	0.195
R_{free}	0.245
RMSD bond lengths (Å)	0.018
RMSD bond angles (°)	1.578
Number of amino acids	291
Cell parameters:	
Space group	P 21 21 2
a (Å)	174.378
b (Å)	62.249
c (Å)	40.732
α	90.0
β	90.0
γ	90.0
Wavelength (Å)	0.979
Total number of reflections	166969
Data redundancy	5.4
⟨I/σ(I)⟩ (highest resolution shell)	13.3 (5.1)
R_{merge} (I)	0.119
R_{sym} (*I*) (highest resolution shell)	0.107 (0.56)
Residues with ideal torsion angles (%)	98
Residues with allowed torsion angles (%)	100

SKs and as a basis to determine the functional implications of sequence variation between AtSK1 and AtSK2. Crystals of the AtSK2 protein were obtained using a truncated construct lacking the N-terminal cTP (residues 1-55). We were unable to crystallize AtSK1; however, we expect the overall structure of AtSK1 and AtSK2 to be essentially identical based on their amino acid sequence identity of ~80% and circular dichroism scans indicating nearly identical secondary structure content for these proteins (Supporting Information Fig. S4). The AtSK2 structure was determined using molecular replacement with the SK structure from *Erwinia chrysanthemi* (Ec) (PDB entry 2SHK; 28% identity with AtSK2) and refined to a resolution of 2.3 Å and a final *R*-factor of 19.5% (R_{free} of 24.5%). The summary of crystallographic statistics is presented in Table I.

AtSK2 belongs to the nucleoside monophosphate kinase family[32] and adopts an α-β-α fold with a central sheet of five parallel β-strands flanked by two layers of α-helices [Fig. 2(A)]. The AtSK2 structure can be divided into four domains [Fig. 2(B)]: the reduced CORE (RC) domain comprising the central β-sheet and flanking α-helices, the nucleotide binding (NB) domain, which includes the phosphate binding loop (P-loop/Walker-A motif), the disordered LID domain, which contains catalytic and substrate binding residues, and the extended shikimate binding (ESB) domain, which includes a modified SK-type Walker B motif and several other substrate binding residues. Two molecules of AtSK2 crystallized in the asymmetric cell and are nearly identical, with a root mean square deviation (RMSD) of 0.36 Å. The oligomeric organization of the dimer in the asymmetric unit is such that the substrate binding pocket of both molecules are occluded by the loop region between α-helix 3 and α-helix 4 of the adjacent molecule (Supporting Information Fig. S5). Consistent with this observation, we did not find any representative density for ATP in the AtSK2 substrate binding pocket although this substrate was present in the AtSK2 crystallization condition.

Structural alignment of AtSK2 (PDB entry 3NWJ) with the *Mycobacterium tuberculosis* (Mt) SK in the closed state in complex with shikimate and ADP (PDB entry 2IYQ; RMSD = 1.27 Å) illustrates the expected orientation of substrates in the AtSK2

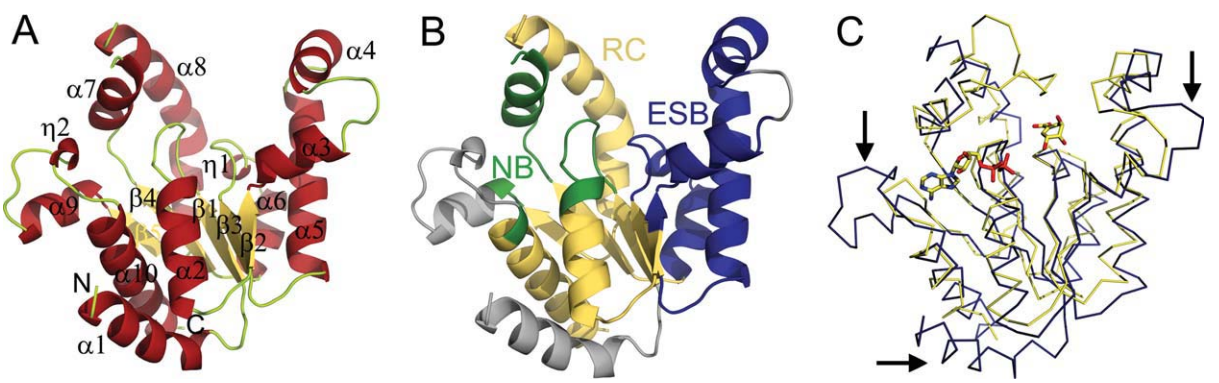

Figure 2. Overall structure of AtSK2. (A) Cartoon diagram of the AtSK2 X-ray crystal structure (PDB entry 3NWJ) depicting secondary structure elements. α-Helices are shown in red, β-strands are shown in yellow-orange, and loop regions are shown in green. (B) Cartoon diagram of AtSK2 (PDB entry 3NWJ) showing the functional SK domains common to bacterial SKs (29) The nucleotide binding (NB) domain is colored green, the RC domain is coloured yellow-orange, and the extended shikimate binding (ESB) domain is coloured blue. (C) C-α ribbon trace of a tertiary alignment of AtSK2 (PDB entry 3NWJ), shown in blue, with the crystal structure of shikimate kinase from Mycobacterium tuberculosis (PDB entry 2IYQ), shown in yellow and in complex with shikimate and ADP rendered as sticks. Black arrows indicate structural features of AtSK2 that are not present in the MtSK structure (Q82-G98, M137-S141, L256-T272). The extended loop region of the LID domain was not modeled in the AtSK2 structure. [Color figure can be viewed in the online issue, which is available at wileyonlinelibrary.com.]

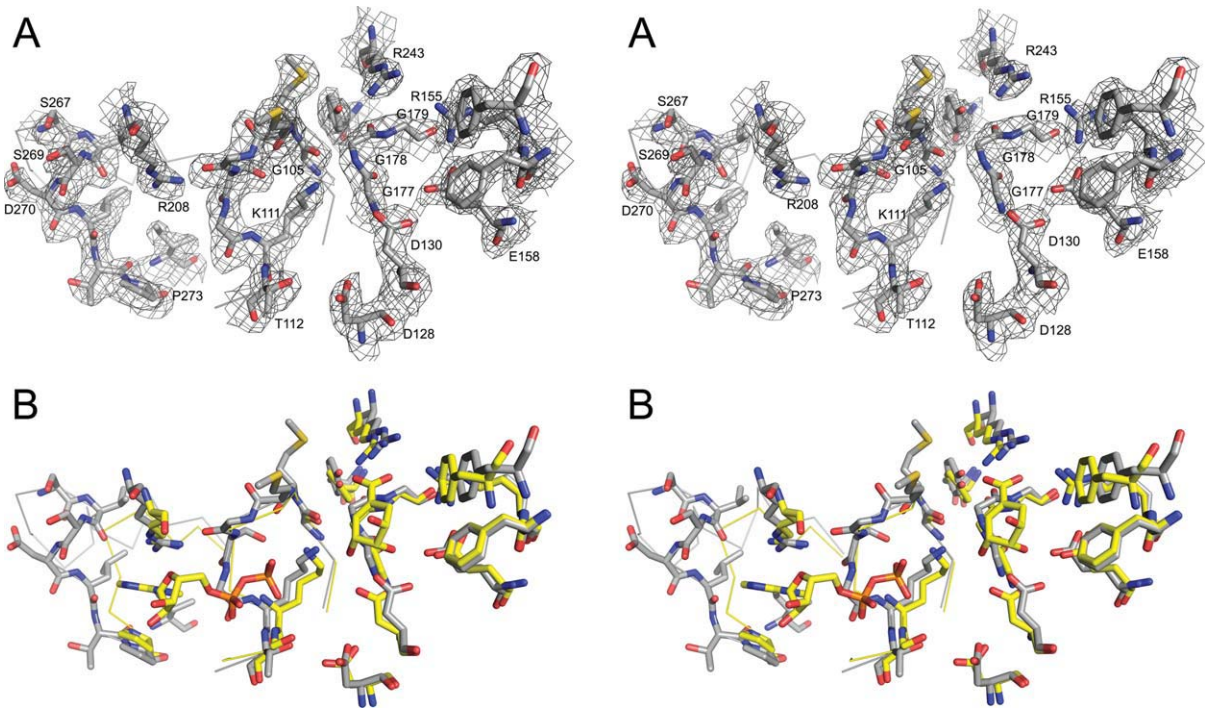

Figure 3. Stereo projection of the AtSK2 substrate binding pocket superimposed with MtSK. (A) The experimental $2F_0$–F_C electron density map contoured at 1.1σ of the AtSK2 crystal structure (PDB entry 3NWJ) is superimposed over the amino acids forming the substrate binding pocket of AtSK2. The key substrate binding residues, as per (65–69), are indicated. (B) The substrate binding residues of AtSK2, as shown as in A), are aligned with the substrate binding residues and the bound ADP and shikimate molecules of the closed MtSK structure (PDB entry 2IYQ) shown in yellow. The P-loop domains and the novel AtSK2 domain between β-strand 5 and the C-terminal α-helix 10 are shown as C-α ribbon traces. The hydrogen bond distance between the backbone carbonyl group of S267 and the amino group of D270 in 3_{10}-helix 2 is 3.0 A. [Color figure can be viewed in the online issue, which is available at wileyonlinelibrary.com.]

active site [Fig. 2(C)]. The apo-AtSK2 structure adopts the open conformation,[29,30] as indicated by the orientation of the disordered LID domain away from the active site and the spacing of the ESB and NB domains away from the RC domain relative to the closed conformation MtSK structure. The AtSK2 structure aligns to the open conformation MtSK structure (PDB entry 2IYT) with RMSD of 1.12 Å. Comparison of AtSK2 with bacterial structures reveals novel features specific to plant SKs [Fig. 2(C)]. The N-terminal α-helix 1 of AtSK2 is not found in bacterial SKs (Fig. 1). There are 28 residues preceding α-helix 1, which were not built in the AtSK2 structure due to a lack of corresponding electron density. An additional novel structural feature of AtSK2 is an extended loop region between α-helix 3 and α-helix 4. This region is known to rotate into the active site on substrate binding.[29,30] If the three AtSK2 structural features not found in bacterial SKs, indicated by arrows in Figure 2(C), are removed from the AtSK2 structure, the RMSD of tertiary alignment with MtSK (PDB entry 2IYT) is essentially unchanged at 1.10 Å. Most of the AtSK2 LID domain between α-helix 7 and α-helix 8 (residues 212-227) was not modeled in the AtSK2 crystal structure due to a lack of corresponding electron density. This region contains the substrate binding and putatively catalytic arginine (Arg117) of the LID domain[26] (Fig. 1). The unresolved AtSK2 LID domain is several residues larger than the EcSK and MtSK LID domains (Fig. 1). The AtSK2 substrate binding pocket is well ordered and highly conserved with the MtSK-crystal structure (Fig. 3). The important SK substrate binding residues reported from bacterial SKs[28–30] are conserved in the AtSK2 structure [Fig. 3(B)]. The aligned AtSK2 NB residues include the adenine binding residues Arg208 and Pro273, the P-loop residues Gly105, Lys111, and the Mg^{2+} coordinating residues Thr112 and Asp128. The aligned AtSK2 shikimate binding residues include Gly177, Gly178, Gly179, and Asp130 of the Walker B motif and Phe146, Phe154, Glu158, Arg155, and Arg243. Although most of the NB residues are conserved, there are distinct differences in the structural features of the NB pocket between the plant and bacterial enzymes. The adenine binding site of AtSK2 is much larger than the bacterial counterpart (Fig. 3). This region is between β-strand 5 and the C-terminal α-helix 10 consisting of α-helix 9, 3_{10}-helix 2, and two loop regions. The 3_{10}-helix 2 contains a serine residue (Ser269), conserved in the *Brassicaceae* SKs (Supporting Information Fig. S6), and is predicted with high probability to be a phosphorylation site based on NetPhos 2.0 (score = 0.99)[34] and Scansite 2.0 (z-score = −2.63).[35]

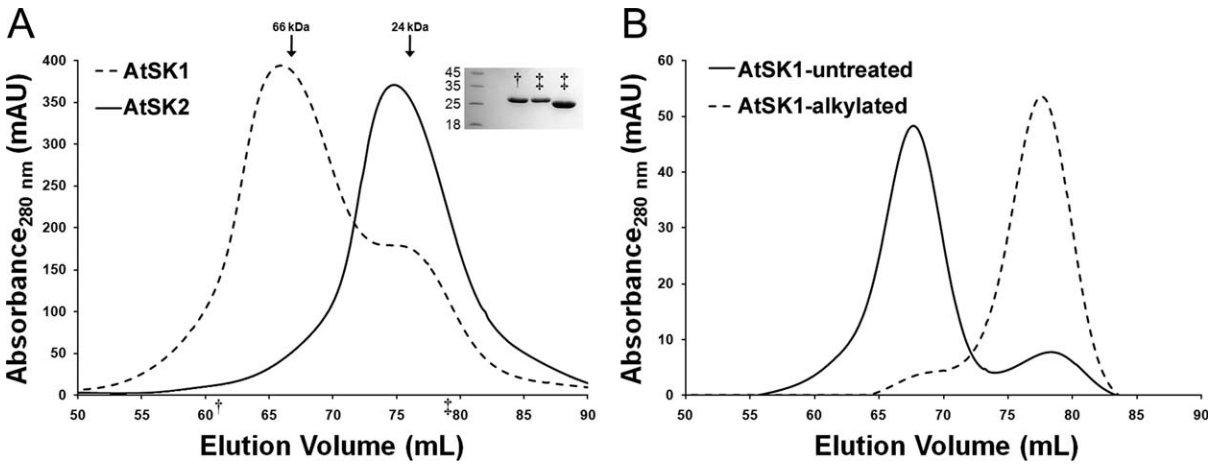

Figure 4. AtSK1 forms a homodimer. (A) Overlay of size exclusion chromatography profiles of recombinant AtSK1 and AtSK2. The expected molecular weight of AtSK1 monomer is 27.8 kDa, and AtSK2 monomer 27.5 kDa. The elution volumes and molecular weights of bovine serum albumin (66 kDa) and AtSKL1-64 (24 kDa) are depicted with vertical arrows above the curves. The inset SDSPAGE analysis shows Coomassie staining of elution fractions of AtSK1 at 61 mL (†) and AtSK1 and AtSK2 at 79 mL (‡). Sizes of molecular weight standards (Fermentas #SM0431) are indicated. (B) Overlay of size exclusion chromatography profiles of the dimer form of recombinant AtSK1 recovered from the purification shown in A). The solid line trace shows the elution profile of the untreated AtSK1 dimer. The dashed line trace shows the elution profile of AtSK1 treated with the reducing agent dithiotreitol and alkylated with iodoacetamide.

AtSK1 forms a homodimer and remains active under heat stress

We assessed the biophysical properties of recombinantly produced AtSK1 and AtSK2 *in vitro*. These recombinant proteins are ~80% identical and their molecular weights (AtSK1 = 27.8 kDa; AtSK2 = 27.5 kDa) are consistent with those of native SKs (27–31 kDa) purified from plant chloroplasts.[11,12] We can reasonably expect these recombinant constructs of AtSK1 and AtSK2 to reflect their native conformations *in vivo*. Size exclusion chromatography indicates AtSK1 exists mainly as a homodimer, eluting at approximately 56 kDa [Fig. 4(A)]. Although two molecules were found in the asymmetric unit of the AtSK2 crystal structure, AtSK2 is a monomer in solution [Fig. 4(A)]. Circular dichroism analysis indicates that the secondary structure of AtSK1 and AtSK2 are highly similar and that both the monomeric and dimeric species of AtSK1 adopt a similar fold (Supporting Information Fig. S4). The homodimeric form of AtSK1 can be recovered following subsequent size exclusion chromatography. AtSK1 has a cysteine (Cys67) in the disordered region preceding the N-terminal α-helix 1. This residue is absent from the *Brassicaceae* SK2 sequences but is conserved in the *Brassicaceae* SK1 sequences (Fig. 1). Both AtSK1 and AtSK2 have a cysteine residue between the two aspartates of the SK-type Walker B motif (Fig. 1). Reduction and cysteine-alkylation of the dimeric form of AtSK1 stabilizes the monomeric species of this enzyme [Fig. 4(B)]. This suggests the N-terminal Cys67 of AtSK1 is likely required for dimer formation. Alkylation causes a minor reduction of AtSK1 activity but does not modify AtSK2 activity (Supporting Information Fig. S7).

We assessed the activity and stability of recombinant AtSK1 and AtSK2 at 37°C *in vitro*. Stock solutions of recombinant AtSK1 and AtSK2 were prepared at 1 mg/mL and subjected to a time series of incubation at 37°C. We chose this temperature for consistency with heat stress experiments in Arabidopsis,[36,37] and we reasoned that 37°C is expected to be at the extreme range of temperature for the native environment of *Arabidopsis thaliana* Col-0[38] (www.arabidopsis.org). Incubating the untreated monomeric form of AtSK1 at 37°C produces the homodimer species (data not shown). The activity of the AtSK1 and AtSK2 enzymes was assayed spectrophotometrically at 37°C and plotted as a function of incubation time at 37°C [Fig. 5(A)]. AtSK1 maintains over 80% of its activity after several hours of incubation at 37°C. The monomeric alkylated form of AtSK1 loses ~40% of its activity after 1 h at 37°C and gradually loses an additional ~10% activity after 3 h at 37°C. Interestingly, AtSK2 shows a rapid and sustained loss in activity for both the untreated and alkylated form of the enzyme. Toward understanding the mechanism of inactivation of AtSK2, we investigated the effect of heating on the proportion of natively folded AtSK1 and AtSK2 by centrifuging the heated stock solutions at 12,000 *g* for 5 min followed by measurement of the concentration of enzyme in the supernatant as a function of time heated at 37°C [Fig. 5(B)]. Both alkylated and nonalkylated AtSK2 samples aggregated rapidly at 37°C with less than 20% soluble

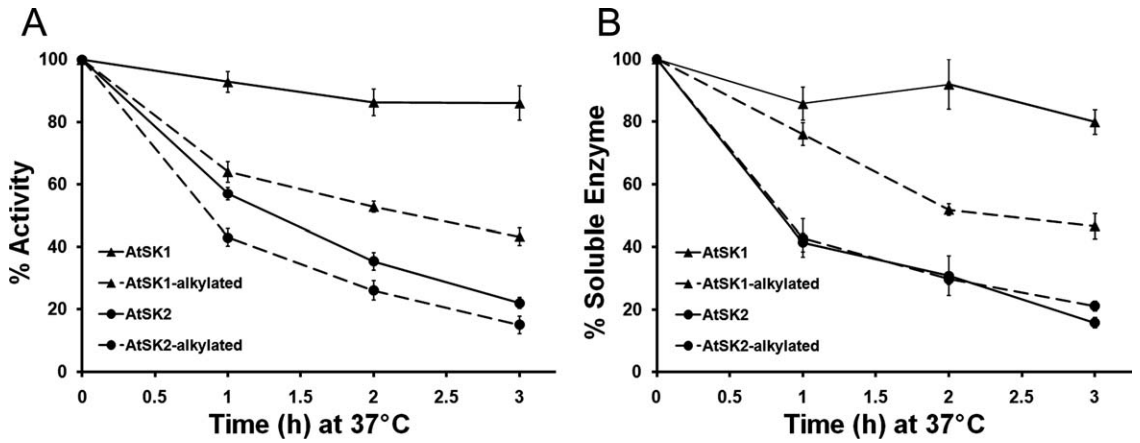

Figure 5. AtSK1 remains active and soluble under prolonged exposure to 37°C. (A) Plot of enzyme activity of recombinant AtSK1 and AtSK2 enzymes as a function of time exposed to heat stress at 37°C and represented as a percent of activity measured before incubation at 37°C. Activity measurements were performed at 37°C. Error bars indicate standard deviation of measurements taken from three separate preparations of each enzyme. (B) Plot of soluble enzyme concentration as a function of time incubated at 37°C and represented as a percent of concentration before incubation at 37°C. Error bars indicate standard deviation of measurements taken from three separate preparations of each enzyme.

enzyme remaining at 3 h of incubation. Conversely, about 80% of the dimeric AtSK1 remained soluble during the 3-h incubation at 37°C.

Computational analysis of AtSK1 and AtSK2 structural variation

The observed loss in activity of alkylated AtSK1 at 37°C suggests that the dimeric form of AtSK1 is important for its thermostability. However, the alkylated monomer of AtSK1 is significantly more stable than AtSK2 during prolonged periods of incubation at 37°C. This indicates that, in addition to dimerization, biophysical variations contributed to the observed stability of AtSK1. There is no significant difference in the overall distribution of side chain properties between the AtSK1 and AtSK2 sequences (without cTP residues) (Supporting Information Table S1). Figure 6(A) shows the variant sites between AtSK1 and AtSK2 on the AtSK2 crystal structure model. All of these variant sites are solvent accessible, and much of this variation clusters to one surface of the AtSK2 structure [Fig. 6(A), right panel].

We calculated which AtSK1 variant sites are likely to confer stability relative to AtSK2 using a computational analysis of the effect of substituting AtSK2 residues to corresponding AtSK1 variants on the ground state stabilization energy of AtSK2. We used the PREDMUT algorithm, which was shown to accurately predict which mutations of the p53 tumor suppressor gene confer stabilizing and destabilizing effects to the encoded protein.[39] Figure 6(B) illustrates the predicted effects of mutation to each residue of AtSK2. The average ground state energy of the molecule as a result of each of the 19 possible mutations at each position is displayed colorimetrically, red indicates a stabilizing effect, that is, a movement from higher to lower ground state energy for the protein molecule when a substitution is made, conversely green indicates a destabilizing effect for substitution at the indicated position of the protein. The β-sheet of the RC domain and the P-loop of AtSK2 are highly stable and almost all mutations to these regions are destabilizing. The novel helical and loop region between β strand-5 and the C-terminal helix-10 is also particularly sensitive to mutation. The calculated energies for each of the AtSK1 site variant mutations of AtSK2 are shown in Supporting Information Table S2. Seventy percent of these mutations are predicted to have a stabilizing effect on the AtSK2 structure. Figure 6(C) illustrates the calculated energies for the SK1 variant mutations on the AtSK2 crystal structure model. The predicted stabilizing effects of AtSK1 mutations relative to AtSK2 can be evaluated against the AtSK2 structure. For example, Ala119 of AtSK2 is in a highly solvated area surrounded by predominantly polar groups. The AtSK1 variant at this position is a serine, which we expect would be more stable in this position and is also predicted to confer a lower ground state energy (−15.5 kcal/mol) relative to the AtSK2 alanine variant. Similarly, Ser121 of the AtSK2 structure is surrounded by hydrophobic residues; therefore, the energetics of accommodating this polar residue in a hydrophobic environment is high. The AtSK1 variant at this position is valine, which we would also expect to be stabilizing and is consistent with the lower calculated energy for this mutation (−10.2 kcal/mol). This is consistent with substituting other hydrophobic residues at this position, almost all of which are predicted to have a stabilizing effect. Other AtSK1 mutations relative to

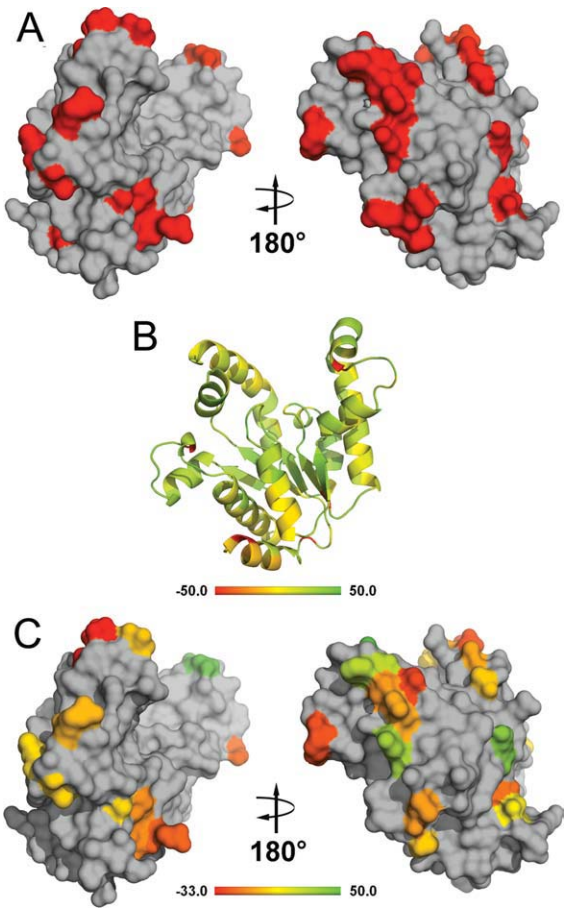

Figure 6. Computational analysis of sequence variation between AtSK1 and AtSK2. (A) Variant amino acid sites between AtSK1 and AtSK2 sequences (shown in red) are mapped onto the AtSK2 crystal structure model. Two sides of the molecule are shown with a rotation of 180° around the *y*-axis. (B) Each position of the AtSK2 crystal structure is colored according to the average difference in energy between the native AtSK2 structure and each of the 19 possible amino acid mutations. Red indicates high energy residues which on average resulted in lower energies upon mutation, and green indicates low energy residues which on average resulted in higher energies on mutation. The scale bar represents calculated difference in energy in kcal/mol. (C) The variant sites indicated in (A) are colored according to calculated energy for the AtSK1 mutations relative to the native AtSK2 structure. [Color figure can be viewed in the online issue, which is available at wileyonlinelibrary.com.]

AtSK2 are predicted to confer substantial stabilizing effects, including K87R, R120K, K138N, S152N, T230S, L233F, N234K, and S251N.

Discussion

The AtSK2 crystal structure demonstrates that the general SK active site architecture is highly conserved between plants and microbes. This is consistent with the observed patterns of strong purifying selection among plant SK genes.[14] Comparison of the AtSK2 structure with the MtSK structure identified features which are conserved among plants but absent from microbial SKs and may facilitate distinct regulatory mechanisms in the plant protein (Figs. 2–3). Based on their high sequence identity, we expect that the AtSK1 protein structure is nearly identical to AtSK2. However, the biophysical properties of AtSK1 are distinct from AtSK2. Specifically, AtSK1 forms a homodimer and remains stable during prolonged exposure to 37°C. The N-terminal Cys67 of AtSK1, conserved across the Brassicaceae SK1 sequences, is likely required for AtSK1 dimerization. Cys67 is the only cysteine unique to AtSK1 compared to AtSK2, and alkylation prevents the dimerization of AtSK1 (Fig. 4). The second AtSK1 cysteine is unlikely to participate in an intermolecular disulfide bond, as the side-chain of the equivalent cysteine in the AtSK2 structure (Cys129) is oriented toward the hydrophobic core of the protein. It is reasonable to assume that the equivalent AtSK1 residue is equally unlikely to form a disulfide bond due to the high sequence identity between AtSK1 and AtSK2 and the adjacency of Cys129 to Mg^{2+} and shikimate binding residues (Asp128, Asp130), which would disfavor significant reorientation in the AtSK1 structure. The observed loss in activity of alkylated AtSK1 at 37°C suggests that the dimeric form of AtSK1 is important for its thermostability (Fig. 5). It is known that heat stress induces the formation of oxidizing compounds *in planta*,[40,41] which could favor the formation of AtSK1 homodimers. Although the AtSK1 homodimer is clearly important for the relative of stability of AtSK1 compared to AtSK2, the alkylated monomer of AtSK1 remains significantly more stable than AtSK2 at prolonged periods of incubation at 37°C. This indicates that additional sequence variation contributes to the observed stability of AtSK1. Our computational analysis predicts that most of the AtSK1 site variants confer stabilization by lowering the ground state energy of the protein (Supporting Information Table S2). The region of clustered variation [Fig. 6(A)] could also be involved in facilitating the formation of stable AtSK1 homodimers. However, these *in silico* predictions require experimental validation through site-directed mutagenesis. Taken together, our data suggests that the stability of AtSK1 relative to AtSK2 is primarily due to its ability to form a homodimer through a disulfide bond. We propose that AtSK1 thermostability maintains shikimate pathway flux during extended periods of heat stress when AtSK2 is likely to be inactivated. Explicit tests of the structural basis for the functional asymmetry between AtSK1 and AtSK2 will require mutagenesis of the variant AtSK1 and AtSK2 sites and Cys67 of AtSK1 in addition to analyses of an experimental model of the three-dimensional AtSK1 structure.

The ability of an enzyme in a high-flux pathway to resist inactivation under conditions of increased flux demand is a plausible basis for adaptive

evolution and is consistent with the observed functional association of AtSK1 with stress response genes (Supporting Information Fig. S3). Asymmetric diversification of gene expression among plant gene duplicates associated with stress responses have an elevated probability of retention and are, therefore, likely to play a role in adaptive evolution.[42] The clustering of monocot SKs from multiple species in distinct clades indicates the occurrence of ancient SK gene duplications that have been conserved within the monocot family for ~140 million years.[43] The half-life to silencing and loss of duplicate genes in Arabidopsis has been approximated to 20 million years.[44] This suggests that SK gene duplicate retention serves adaptive functions across the plant kingdom. However, the lineage-specific emergence and retention of SK isoforms in plants predicts that the underlying mechanisms for the retention of these isoforms are similarly lineage specific. The induction of AtSK1 gene expression under heat stress and the ability of the AtSK1 protein to retain its activity following prolonged periods of incubation at 37°C suggest a functional correlation between the regulation of AtSK1 and AtSK2 gene expression and the structure and function of the encoded proteins. Further experiments are required to demonstrate that a coevolutionary process underlies the correlation of the heat stress induction of AtSK1 gene expression and the thermostability of the encoded protein. For example, the conservation of SK1 dimerization and thermostability could be evaluated in other Brassicaceae species. Differences in shikimate pathway flux could also be evaluated in null mutants of AtSK1 and AtSK2, which could be screened for metabolic or growth phenotypes in response to heat stress. The abundance of shikimate is an important parameter in balancing shikimate pathway flux to demands for stress responses, growth, and development. For example, plant acyltransferases that accept either shikimate or quinate for esterification with *p*-Coumaroyl-CoA can regulate shikimate pathway flux to the production of lignin, chlorogenic acid, or important volatile compounds.[16,45,46] The spatiotemporal regulation of SK isoforms with distinct kinetic properties may, therefore, contribute to partitioning of shikimate pathway flux by controlling the steady state abundance of shikimate.

Materials and Methods

Protein expression and purification

AtSK1 and AtSK2 coding sequences were cloned as per Reference 14. These constructs were designed based on *in silico* predictions of cTP lengths,[47] secondary structure predictions,[48] and sequence conservation within an orthologous set of plant SKs as per Reference 14. Both AtSK1 and AtSK2 recombinant constructs were designed to remove residues 1-55 from the N-terminus. Total cellular RNA was extracted from 10-day-old *Arabidopsis thaliana* Col-0 seedlings using TRIzol Reagent (Invitrogen) and cDNA was prepared using poly-dT primers and SuperScript II (Invitrogen). Coding sequences were amplified from this cDNA using the designed primers. PCR products were digested with NdeI and BamHI and ligated into pET15b. The AtSK1 and AtSK2 expression constructs were transformed into BL21 *E. coli* cells for expression with the IPTG-inducible T7 system. The recombinant enzymes were purified using Ni-NTA chromatography. Eluted proteins were dialyzed against a Tris buffer (10 m*M* 2-amino-2-hydroxymethyl-propane-1,3-diol (Tris) pH 8.0, 150 m*M* NaCl, and 2 m*M* dithiotreitol). Hexahistidine tags were cleaved from the recombinants with thrombin. Removal of the His-tags was confirmed by sodium dodecyl sulfate polyacrylamide gel electrophoresis. Recombinant AtSK1 and AtSK2 were further purified by Ni-NTA chromatography to remove the His-tags followed by size exclusion chromatography. The latter was performed on a Superdex S-200 column (GE Healthcare) with a mobile phase of 150 m*M* NaCl and 10 m*M* Tris buffer (pH 8.0) at a rate of 1 mL/min. Recombinant protein (20 mg) was loaded for the size exclusion chromatography shown in Figure 4(A).

AtSK2 crystallization and structure determination

Recombinant AtSK2 was crystallized at room temperature using the hanging drop, vapor-diffusion method at 3 mg/mL mixed 1:1 with a solution of 22% polyethylene glycol 3350, 0.2*M* potassium fluoride, 3% 2-methyl-2,4-pentanediol, 1 m*M* magnesium chloride, and 1 m*M* ATP. The growth rate of crystals varied from 3 days to several weeks. Crystals were transferred into cryoprotectant solution (22% glycerol suspended in the mother liquor solution of the crystal) and flash-frozen in liquid nitrogen. Initial characterization of the protein crystals was conducted on a MicroMax 007-HF generator equipped with Saturn 944+ CCD detector at a local X-ray source. X-ray diffraction data were collected from a single crystal at 100 K in a nitrogen stream at beamline ID19 at the Advanced Photon Source of Argonne National Laboratory with an ADSC 914 detector system. The diffraction data were processed in the space group P21212 using XDS[49] and scaled using SCALA from the CCP4 suite.[50] The structure was solved by molecular replacement with SK from Ec (PDB entry 2SHK) after editing with Chainsaw (CCP4 suite) associated with MOLREP.[51] Resolution range (19.0–2.35) and the number of molecules expected (2, Matthews coefficient of 2.05 $Å^3$/Da and a solvent content of 39.95%) in the asymmetric unit were fixed for the phasing procedure. The first restrained refinement using Refmac5[52] confirmed the quality of the determined solution (initial

R_{free} = 0.493, final R_{free} = 0.448 after 30 cycles). The model was further modified by AutoBuild from the PHENIX suite[53] (R_{free} = 0.356) and completed by iterative cycles of refinement with Coot[54] and Refmac5.[52,55] Forty-four water molecules were positioned in well-defined positive (mF_0-DF_C) residual densities with a lower cutoff of 3σ. Crystallographic model refinement and data collection statistics are presented in Table I. Representative figures of the crystal structure were produced with PyMOL.[56] Tertiary alignments were performed using the "super" function in PyMOL.

Kinetics and biophysical characterization of AtSK1 and AtSK2

SK activity was measured spectrophotometrically as previously described.[14,25] The reaction temperature was controlled with a Peltier device attached to the UV–vis spectrophotometer (Cary). Extinction coefficients of 30,035 M^{-1} cm^{-1} and 29,910 M^{-1} cm^{-1} at 280 nm were used for determining the concentration of highly purified recombinant AtSK1 and AtSK2, respectively, as calculated by ProtParam (www.expasy.ch/tools/protparam.html). Circular dichroism measurements were performed using a Jasco J-810 spectropolarimeter at 25°C with AtSK1 and AtSK2 at a concentration of 20 μ*M* in 10-m*M* sodium phosphate (pH 7.5) and 150-m*M* sodium chloride. Size exclusion chromatography was performed on a Superdex S-200 column (GE Healthcare) with a mobile phase of 150-m*M* NaCl and 10-m*M* Tris (pH 8.0) at a rate of 1 mL/min. Similar retention times for AtSK1 and AtSK2 were observed with a mobile phase of 500-m*M* NaCl and 10-m*M* Tris (pH 8.0). Cysteine-alkylation was performed by first reducing the enzymes with 2.5-m*M* dithiotreitol, followed by dialysis in 10-m*M* Tris (pH 8.0) and 150-m*M* NaCl, followed by concentrating the enzymes to 0.3 μM and cysteine-alkylation with the addition of 10-m*M* iodoacetamide and incubation at room temperature for 30 min. Following alkylation, the enzymes were repurified by size exclusion chromatography.

Computational analysis of SK1/SK2 sequence variation and stability

The stability parameter in the PREDMUT algorithm[39] was used to predict the difference in calculated energy between the native AtSK2 crystal structure (PDB entry 3NWJ, molecule A only) and each of the 19 possible amino acid mutations at every site of the AtSK2 structure. Calculated energies were determined by the minimum energy from four simulation runs for each mutation using ICM, Molsoft Inc.[57,58] Colorimetric displays of energy calculations were prepared by incorporating these measurements into the B-factor field of the AtSK2 PDB file using a Perl script and rendering the color scale in PyMOL with the "Spectrumbar" Python script (http://pymolwiki.org/index.php/spectrumbar). Differences in calculated energy were summed with a midpoint of 50 for the B-factor field, indicating no change in calculated energy. Calculated energy differences exceeding 50 kcal/mol were fixed to 0 and 100 for high-energy and low-energy positions, respectively.

Acknowledgments

The authors thank Pierre Petit for his assistance in obtaining initial phases for the AtSK2 crystal structure and Vivian Saridakis for providing access to the X-ray generator facilities at York University. Results shown in this report are derived from work performed at Argonne National Laboratory, Structural Biology Center at the Advanced Photon Source. Argonne is operated by UChicago Argonne, LLC, for the U.S. Department of Energy, Office of Biological and Environmental Research under contract DE-AC02-06CH11357. The authors thank Younchang Kim at beamline 19ID for assistance in X-ray diffraction data collection. The authors acknowledge support from the Center for the Analysis of Genome Evolution and Function.

References

1. Herrmann KM, Weaver LM (1999) The shikimate pathway. Annu Rev Plant Physiol Plant Mol Biol 50: 473–503.
2. Tzin V, Galili G (2010) New insights into the shikimate and aromatic amino acids biosynthesis pathways in plants. Molecular Plant 3:956–972.
3. Herrmann KM (1995) The shikimate pathway as an entry to aromatic secondary metabolism. Plant Physiol 107:7–12.
4. Floss HG (1997) Natural products derived from unusual variants of the shikimate pathway. Nat Prod Rep 14:433–452.
5. Roberts F, Roberts CW, Johnson JJ, Kyle DE, Krell T, Coggins JR, Coombs GH, Milhous WK, Tzipori S, Ferguson DJ, Chakrabarti D, McLeod R (1998) Evidence for the shikimate pathway in apicomplexan parasites. Nature 393:801–805.
6. Keeling PJ, Palmer JD, Donald RG, Roos DS, Waller RF, McFadden GI (1999) Shikimate pathway in apicomplexan parasites. Nature 397:219–220.
7. Campbell SA, Richards TA, Mui EJ, Samuel BU, Coggins JR, McLeod R, Roberts CW (2004) A complete shikimate pathway in *Toxoplasma gondii*: an ancient eukaryotic innovation. Int J Parasitol 34:5–13.
8. Richards TA, Dacks JB, Campbell SA, Blanchard JL, Foster PG, McLeod R, Roberts CW (2006) Evolutionary origins of the eukaryotic shikimate pathway: gene fusions, horizontal gene transfer, and endosymbiotic replacements. Eukaryot Cell 5:1517–1521.
9. Starcevic A, Akthar S, Dunlap WC, Shick JM, Hranueli D, Cullum J, Long PF (2008) Enzymes of the shikimic acid pathway encoded in the genome of a basal metazoan, *Nematostella vectensis*, have microbial origins. Proc Natl Acad Sci USA 105:2533–2537.
10. Steinrucken HC, Amrhein N (1980) The herbicide glyphosate is a potent inhibitor of 5-enolpyruvyl-shikimic acid-3-phosphate synthase. Biochem Biophys Res Commun 94:1207–1212.

11. Schmidt CL, Danneel HJ, Schultz G, Buchanan BB (1990) Shikimate kinase from spinach chloroplasts: purification, characterization, and regulatory function in aromatic amino acid biosynthesis. Plant Phys 93: 758–766.
12. Schmid J, Schaller A, Leibinger U, Boll W, Amrhein N (1992) The *in-vitro* synthesized tomato shikimate kinase precursor is enzymatically active and is imported and processed to the mature enzyme by chloroplasts. Plant J 2:375–383.
13. Kasai K, Kanno T, Akita M, Ikejiri-Kanno Y, Wakasa K, Tozawa Y (2005) Identification of three shikimate kinase genes in rice: characterization of their differential expression during panicle development and of the enzymatic activities of the encoded proteins. Planta 222: 438–447.
14. Fucile G, Falconer S, Christendat D (2008) Evolutionary diversification of plant shikimate kinase gene duplicates. PLoS Genet 4:e1000292.
15. Görlach J, Raesecke HR, Rentsch D, Regenass M, Roy P, Zala M, Keel C, Boller T, Amrhein N, Schmid J (1995) Temporally distinct accumulation of transcripts encoding enzymes of the prechorismate pathway in elicitor-treated, cultured tomato cells. Proc Natl Acad Sci USA 92:3166–3170.
16. Hoffmann L, Maury S, Martz F, Geoffroy P, Legrand M (2003) Purification, cloning, and properties of an acyltransferase controlling shikimate and quinate ester intermediates in phenylpropanoid metabolism. J Biol Chem 278:95–103.
17. Blanc G, Hokamp K, Wolfe KH (2003) A recent polyploidy superimposed on older large-scale duplications in the Arabidopsis genome. Genome Res 13: 137–144.
18. Kilian J, Whitehead D, Horak J, Wanke D, Weinl S, Batistic O, D'Angelo C, Bornberg-Bauer E, Kudla J, Harter K (2007) The AtGenExpress global stress expression data set: protocols, evaluation and model data analysis of UV-B light, drought and cold stress responses. Plant J 50:347–363.
19. Forreiter C, Nover L (1998) Heat stress-induced proteins and the concept of molecular chaperones. J Biosci 23:287–302.
20. Beggs CJ, Kuhn K, Böcker R, Wellmann E (1987) Phytochrome-induced flavonoid biosynthesis in mustard (*Sinapis alba* L.) cotyledons: enzymic control and differential regulation of anthocyanin and quercetin formation. Planta 172:121–126.
21. Dixon RA, Paiva NL (1995) Stress-induced phenylpropanoid metabolism. Plant Cell 7:1085–1097.
22. Rivero RM, Ruiz JM, García PC, López-Lefebre LR, Sánchez E, Romero L (2001) Resistance to cold and heat stress: accumulation of phenolic compounds in tomato and watermelon plants. Plant Sci 5:315–321.
23. Li WH, Yang J, Gu X (2005) Expression divergence between duplicate genes. Trends Genet 11:602–607.
24. Shakhnovich BE, Shakhnovich EI (2008) Improvisation in evolution of genes and genomes: whose structure is it anyway? Curr Opin Struct Biol 18:375–381.
25. Krell T, Maclean J, Boam DJ, Cooper A, Resmini M, Brocklehurst K, Kelly SM, Price NC, Lapthorn AJ, Coggins JR (2001) Biochemical and X-ray crystallographic studies on shikimate kinase: the important structural role of the P-loop lysine. Protein Sci 10: 1137–1149.
26. Gu Y, Reshetnikova L, Li Y, Wu Y, Yan H, Singh S, Ji X (2002) Crystal structure of shikimate kinase from *Mycobacterium tuberculosis* reveals the dynamic role of the LID domain in catalysis. J Mol Biol 319:779–789.
27. Dhaliwal B, Nichols CE, Ren J, Lockyer M, Charles I, Hawkins AR, Stammers DK (2004) Crystallographic studies of shikimate binding and induced conformational changes in *Mycobacterium tuberculosis* shikimate kinase. FEBS Lett 574:49–54.
28. Cheng WC, Chang YN, Wang WC (2005) Structural basis for shikimate-binding specificity of Helicobacter pylori shikimate kinase. J Bacteriol 187:8156–8163.
29. Gan J, Gu Y, Li Y, Yan H, Ji XJ (2006) Crystal structure of *Mycobacterium tuberculosis* shikimate kinase in complex with shikimic acid and an ATP analogue. Biochemistry 45:8539–8545.
30. Hartmann MD, Bourenkov GP, Oberschall A, Strizhof N, Bartunik HD (2006) Mechanism of phosphoryl transfer catalyzed by shikimate kinase from *Mycobacterium tuberculosis*. J Mol Biol 364:411–423.
31. Ely B, Pittard J. (1979) Aromatic amino acid biosynthesis: regulation of shikimate kinase in *Escherichia coli* K-12. J Bacteriol 138:933–943.
32. Yan H, Tsai MD (1999) Nucleoside monophosphate kinases: structure, mechanism, and substrate specificity. Adv Enzymol Relat Areas Mol Biol 73:103–134.
33. Blom N, Gammeltoft S, Brunak S (1999) Sequence- and structure-based prediction of eukaryotic protein phosphorylation sites. J Mol Biol 294:1351–1362.
34. Obenauer JC, Cantley LC, Yaffe MB (2003) Scansite 2.0: proteome-wide prediction of cell signalling interactions using short sequence motifs. Nucleic Acids Res 31:3625–3641.
35. Jenkins ME, Suzuki TC, Mount DW (1997) Evidence that heat and ultraviolet radiation activate a common stress-response program in plants that is altered in the uvh6 mutant of *Arabidopsis thaliana*. Plant Physiol 115:1351–1358.
36. Charng YY, Liu HC, Liu NY, Chi WT, Wang CN, Chang SH, Wang TT (2007) A heat-inducible transcription factor, HsfA2, is required for extension of acquired thermotolerance in Arabidopsis. Plant Physiol 143: 251–262.
37. O'Kane SL, Al-Shehbaz IA (1997) A synopsis of Arabidopsis (*Brassicaceae*). Novon 7:323–327.
38. Carlsson J, Soussi T, Persson B (2009) Investigation and prediction of the severity of p53 mutants using parameters from structural calculations. FEBS J 276: 4142–4155.
39. Vacca RA, de Pinto MC, Valenti D, Passarella S, Marra E, De Gara L (2004) Production of reactive oxygen species, alteration of cytosolic ascorbate peroxidase, and impairment of mitochondrial metabolism are early events in heat shock-induced programmed cell death in tobacco Bright-Yellow 2 cells. Plant Physiol 134: 1100–1112.
40. Allakhverdiev SI, Kreslavski VD, Klimov VV, Los DA, Carpentier R, Mohanty P (2008) Heat stress: an overview of molecular responses in photosynthesis. Photosynth Res 98:541–550.
41. Hanada K, Zou C, Lehti-Shiu MD, Shinozaki K, Shiu SH (2008) Importance of lineage-specific expansion of plant tandem duplicates in the adaptive response to environmental stimuli. Plant Physiol 148:993–1003.
42. Chase MW (2004) Monocot relationships: an overview. Am J Bot 91:1645–1655.
43. Lynch M, Conery JC (2001) Gene duplication and evolution—a response. Science 293:1551.
44. Sonnante G, D'Amore R, Blanco E, Pierri CL, De Palma M, Luo J, Tucci M, Martin C (2010) Novel hydroxycinnamoyl-coenzyme A quinate transferase genes from artichoke are involved in the synthesis of chlorogenic acid. Plant Physiol 153:1224–1238.

45. Gang DR, Beuerle T, Ullmann P, Werck-Reichhart D, Pichersky E (2002) Differential production of meta hydroxylated phenylpropanoids in sweet basil peltate glandular trichomes and leaves is controlled by the activities of specific acyltransferases and hydroxylases. Plant Physiol 130:1536–1544.
46. Emanuelsson O, Nielsen H, von Heijne G (1999) ChloroP, a neural network-based method for predicting chloroplast transit peptides and their cleavage sites. Protein Sci 8:978–984.
47. Kelley LA, Sternberg MJE (2009) Protein structure prediction on the Web: a case study using the Phyre server. Nat Protoc 4:363–371.
48. Kabsch W (1993) Automatic processing of rotation diffraction data from crystals of initially unknown symmetry and cell constants. J Appl Crystallogr 26:795–800.
49. Collaborative Computational Project Number 4. (1994) The CCP4 suite: programs for protein crystallography. Acta Cryst D50:760–763.
50. Vagin A, Teplyakov A (1997) MOLREP: an automated program for molecular replacement. J Appl Crystallogr 30:1022–1025.
51. Murshudov GN, Vagin AA, Dodson EJ (1997) Refinement of macromolecular structures by the maximum-likelihood method. Acta Cryst D53:240–255.
52. Adams PD, Grosse-Kunstleve RW, Hung LW, Ioerger TR, McCoy AJ, Moriarty NW, Read RJ, Sacchettini JC, Sauter NK, Terwilliger TC (2002) PHENIX: building new software for automated crystallographic structure determination. Acta Cryst D58:1948–1954.
53. Emsley P, Cowtan K (2004) Coot: model-building tools for molecular graphics. Acta Cryst D60:2126–2132.
54. Winn MD, Isupov MN, Murshudov GN (2001) Use of TLS parameters to model anisotropic displacements in macromolecular refinement. Acta Cryst D57:122–133.
55. DeLano WL (2002) The PyMOL Molecular Graphics System. San Carlos: DeLano Scientific.
56. Abagyan R, Totrov M (1994) Biased probability Monte Carlo conformational searches and electrostatic calculations for peptides and proteins. J Mol Biol 235:983–1002.
57. Abagyan R, Totrov M, Kuznetsov D (1994) ICM—a new method for protein modeling and design: applications to docking and structure prediction from the distorted native conformation. J Comput Chem 235:983–1002.